International Journal of Nanomedicine Dovepress

Open Access Full Text Article ORIGINAL RESEARCH

Berberine-Loaded PVCL-PVA-PEG Self-Assembled Micelles for the Treatment of Liver Fibrosis

Xiaozhu Zha[1,*], Yumei Hao[2,*], Yifan Ke[1], Yichun Wang[3], Yujia Zhang[2]

[1]Department of Traditional Chinese Medicine, Anqing Medical College, Anqing, People's Republic of China; [2]Beijing Key Laboratory of Drug Delivery Technology and Novel Formulation, Institute of Materia Medica, Chinese Academy of Medical Sciences & Peking Union Medical College, Beijing, 100050, People's Republic of China; [3]Department of Radiation Oncology, the First Affiliated Hospital of Anhui Medical University, Hefei, People's Republic of China

*These authors contributed equally to this work

Correspondence: Yichun Wang; Yujia Zhang, Email wangechun321@sina.com; zhyj@imm.ac.cn

Background: Liver fibrosis is a necessary pathological process in many chronic liver diseases. Studies have shown that the progression of chronic liver disease can be slowed by rational intervention in hepatic fibrosis. Berberine (BBR), a natural extract of Phellodendron amurense, inhibits the development of liver fibrosis through several mechanisms. However, the clinical application of BBR is limited due to its low solubility. Drug delivery systems have been developed to improve the solubility of hydrophobic drugs and increase their efficacy in treating the liver fibrosis.

Methods: In this study, a biocompatible nanomicelle was constructed by thin-film dispersion method using polyvinyl caprolactam-polyvinyl acetate-polyethylene glycol graft copolymer (PVCL-PVA-PEG) as a carrier to encapsulate BBR (PVCL-PVA-PEG/BBR-MCs) to improve the solubility of BBR and reduce the systemic side effects. The ability to inhibit HSC-T6 cell activation of PVCL-PVA-PEG/BBR-MCs was evaluated in vitro. The anti-hepatic fibrosis effects of PVCL-PVA-PEG/BBR-MCs were investigated in vivo.

Results: PVCL-PVA-PEG/BBR-MCs have a uniform spherical shape with a mean particle size of 60.04 ± 0.027 nm and a potential of 1.49 ± 0.32 mV. It had an encapsulation efficiency of 98.52% ± 0.70 and drug loading content of 6.16% ± 0.04. Compared to free BBR, PVCL-PVA-PEG/BBR-MCs significantly inhibited HSC-T6 cell activation and TGF-β1-induced HSC-T6 cell migration in vitro. In vivo biodistribution experiments showed significantly improved hepatic distribution of PVCL-PVA-PEG/DiD-MCs compared to free DiD, suggesting that PVCL-PVA-PEG micelles enhance the ability of BBR to enter the liver and improve therapeutic efficacy. After treatment, PVCL-PVA-PEG/BBR-MCs significantly improved fibrotic liver structure and reduced collagen deposition in comparison to the CCl_4-treated group; the treatment outcome was more effective than that of the free BBR group.

Conclusion: Our results demonstrate the advantages of encapsulating BBR in PVCL-PVA-PEG micelles and highlight the potential of PVCL-PVA-PEG/BBR-MCs as a therapeutic strategy for the treatment of liver fibrosis.

Keywords: liver fibrosis, berberine, hepatic stellate cells, PVCL-PVA-PEG, drug delivery system

Introduction

Liver fibrosis, a chronic liver disease characterized by hepatocyte morphological changes, extracellular matrix accumulation, intrahepatic obstruction and loss of functional hepatocyte clusters, is now a global public health problem.[1–3] The etiology of liver fibrosis is complex, involving the interaction of multiple cells, mediators and signal pathways.[4] Liver fibrosis is an inevitable pathological process in many chronic liver diseases.[2] If not treated in time, it can lead to cirrhosis or even liver cancer. A number of studies have shown that interventions that target certain cells involved in liver fibrosis can slow down or even reverse the progression of liver fibrosis and can significantly reduce the development of severe chronic liver disease.[5–7] Liver fibrosis is currently being treated by protecting normal liver cells,[8] inhibiting hepatic stellate cells (HSCs) activation,[9] decreasing extracellular matrix synthesis and secretion,[10] and reducing liver inflammation. Interferons (INF; INF-γ),[11] anti-HBV nucleotides and their analogues,[12] endothelin receptor A antagonists,[13,14]

Received: 21 February 2024
Accepted: 17 October 2024
Published: 25 October 2024

Graphical Abstract

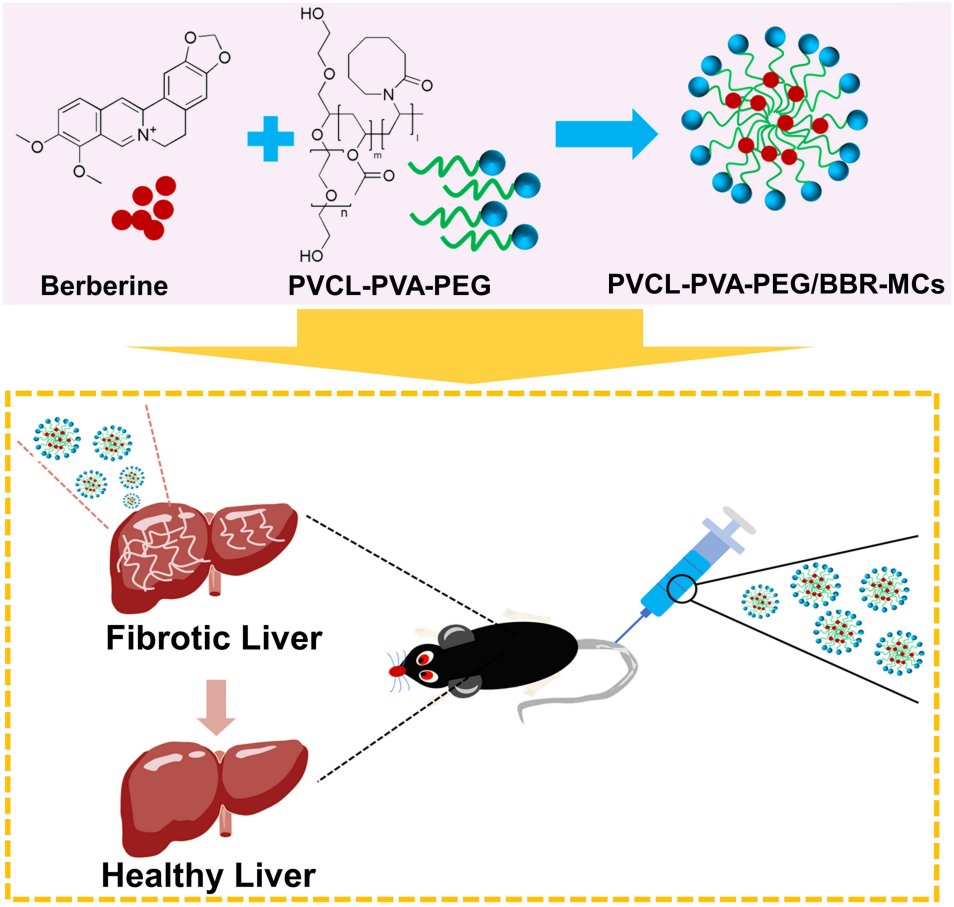

angiotensin receptor blockers, and extracts of natural products such as colchicine[15] and silymarin[16] are commonly used in the treatment of liver fibrosis, with some success. However, the current lack of clinical applications remains.

Berberine (BBR), an isoquinoline alkaloid found in the genus Phellodendron, has a wide range of pharmacological activities including antioxidant, antibacterial, anti-inflammatory, anticancer, anti-diabetic, anti-dyslipidaemic and anti-obesity properties.[17–21] Recent studies have shown that it also plays an important role in the treatment of a wide range of fibrotic diseases such as liver fibrosis,[22,23] lung fibrosis,[24] kidney fibrosis[25,26] and heart fibrosis.[27,28] The metabolic process of BBR consists of two main steps, 1) demethylation, reduction and cleavage of the dioxymethylene in the molecular structure of BBR and 2) glucuronidation, sulfation and methylation.[29] BBR is metabolized in the liver, where it provides the material and structural basis for treating hepatic fibrosis. However, the use of BBR in clinical practice is limited by its extremely low water solubility and bioavailability. To improve its solubility, many studies have attempted to make berberine hydrochloride, which is inevitably damaging to other organs.[30]

PVCL-PVA-PEG (soluplus®), a biocompatible amphiphilic block copolymer, can be used to improve the solubility of hydrophobic drugs.[31,32] It has been reported that soluplus® has a very low critical micelle concentration (CMC) of about 7–8 mg/L, which contributes to the stability of the self-assembled micelles.[31] Previously published studies have reported that soluplus® can be self-assembled into a drug delivery system for the encapsulation of water-insoluble drugs for the treatment of eye diseases and tumours.[33,34]

In this study, based on the perspective that nanodrug delivery systems can improve the solubility and biocompatibility of hydrophobic drugs,[35,36] BBRs were prepared as homogeneously dispersed micelles that can be dissolved in aqueous

solution. To improve berberine bioavailability, we used commercially available PVCL-PVA-PEG as a drug delivery vehicle to encapsulate berberine to prepare PVCL-PVA-PEG/BBR-MCs. The prepared PVCL-PVA-PEG/BBR-MCs improved the solubility of BBR APIs and further enhanced liver accumulation. The therapeutic efficacy of PVCL-PVA-PEG/BBR-MCs on fibrotic liver was evaluated by several physicochemical properties, providing a new potential approach for the treatment of liver fibrosis. The results showed that the prepared PVCL-PVA-PEG/BBR-MCs were efficiently taken up by HSC-T6 cell in vitro. Furthermore, they had a significant inhibitory effect on HSC-T6 cell activation in vitro. In vivo, the results showed that PVCL-PVA-PEG/BBR-MCs were able to reduce collagen deposition, improve the structure of the liver tissue as well as attenuate the progression of liver fibrosis.

Materials and Methods

Materials

Berberine (BBR) and BCA protein assay kit were purchased from Beiing Solarbio Science &Technology Co.Ltd.. Polyvinyl caprolactam-polyvinyl acetate-polyethylene glycol graft copolymer (PVCL-PVA-PEG) was purchased from BASF (CABA, Argentina). HSC-T6 was purchased from Fenghui (Hunan). Dulbecco's Modified Eagle's Medium (DMEM) and fetal bovine serum (FBS) were purchased from Gibco. Alpha-Smooth Muscle antibody was purchased from SIGMA, Anti-Collagen I antibody was purchased from protein technology. DiD, HSP-90, and Tubulin were purchased from Beyotime Biotechnology. CCK-8 kit was purchased from Meilunbio.

Optimization of the Formulation and Characterization of PVCL-PVA-PEG/BBR -MCs

Berberine (BBR)-loaded micelles (PVCL-PVA-PEG/BBR-MCs), were prepared by a thin film dispersion method using PVCL-PVA-PEG as the carrier material. A series of micelles with different BBR/PVCL-PVA-PEG ratios were prepared by fixing the mass of BBR and varying the mass of PVCL-PVA-PEG.

Briefly, BBR and PVCL-PVA-PEG (Mass ratio = 1/3, 1/6, 1/9, 1/12, 1/15, 1/18) were respectively fully dissolved in methanol, and then the methanol was removed by rotary evaporation under vacuum conditions. Finally, the thin films were hydrated with PBS solution. The optimum formulation was established by investigating the size, PDI, entrapment efficiency (EE) and loading content (LC) of the micelles. Similarly, PVCL-PVA-PEG/MCs (blank MCs) were prepared by evaporation of a BBR-free organic solvent containing only PVCL-PVA-PEG under optimal formulation.

Dynamic light scattering (DLS) by Zeta sizer Nano ZS90 instrument (Malvern, UK) was used to measure the mean particle size and zeta potential of (PVCL-PVA-PEG/BBR-MCs). Transmission electron microscopy (TEM; JEM 1200EX, JEOL, Japan) was used to examine the morphology of PVCL-PVA-PEG/BBR-MCs stained with 2% phospho-tungstic acid.

Loading Content and Encapsulation Efficiency of PVCL-PVA-PEG/BBR-MCs

PVCL-PVA-PEG/BBR-MCs were dissolved in methanol and sonicated for 10 min to break up the micelle structure. Briefly, the PVCL-PVA-PEG/BBR-MCs were diluted with methanol, and then the resulting solution was detected by high-performance liquid chromatography (HPLC) to obtain the total amount of added BBR. After that, PVCL-PVA-PEG/BBR-MCs was centrifuged and the same volume as above of supernatant was taken to disrupt the structure with methanol, and the amount of encapsulated BBR was detected by HPLC. Finally, an equal volume of centrifuged supernatant was lyophilized and then weighed to obtain the total weight of the micelles. The loading content (LC) and encapsulation efficiency (EE) of BBR in PVCL-PVA-PEG/MCs could be calculated by the following equation:

$$LC\,(\%) = \frac{W_e}{W_m} \times 100\%$$

$$EE\,(\%) = \frac{W_t - W_f}{W_t} \times 100\%$$

where W_e and W_m are the weight of BBR encapsulated in micelles and the total weight of micelles, respectively; W_t and W_f are the total weight of BBR added and the weight of free BBR not encapsulated in micelles, respectively.

Cell Culture

HSC-T6 cells were cultured in Dulbecco's Modified Eagle's Medium (DMEM) with the addition of 10% fetal bovine serum (FBS), 100 U/mL penicillin, and 100 μg/mL streptomycin, and were incubated at 37 °C with 5% CO_2 atmosphere.

Cytotoxicity Assay of PVCL-PVA-PEG/BBR-MCs and Free BBR

To investigate the viabilities of PVCL-PVA-PEG on normal HSC-T6 cells, the cytotoxicity of PVCL-PVA-PEG/ BBR-MCs to HSC-T6 cells was determined by CCK-8 assays. Briefly, HSC-T6 cells were first seeded into 96-well plates at a density of 1×10^4 cells/well and incubated in 200 μL of DMEM medium containing 10% FBS at 37 °C under 5% CO_2 for 24h. After 24h, HSC-T6 cells were treated with different concentrations (0.9375–120μM) of free BBR, blank MCs and PVCL-PVA-PEG/BBR-MCs for 48 h. At the end of the incubation, 100μL of CCK-8 solution was added to each well to replace the drug medium and incubated for 2h. Finally, the absorbance was measured at 450 nm using a microplate reader (Bio-Rad, United States) to determine the cell viability (%) of each group at different concentrations.

HSC-T6 Cell Uptake Assay of PVCL-PVA-PEG/BBR-MCs

Coumarin 6 (Cou6) was used as a fluorescent probe to investigate the cellular uptake of Cou6-loaded PVCL-PVA-PEG micelles (PVCL-PVA-PEG/Cou6-MCs) by HSC-T6 cells. Fluorescence microscopy (Olympus, Tokyo, Japan) and flow cytometry were used to detect intracellular Cou6 intensity. PVCL-PVA-PEG/Cou6-MCs were prepared according to the preparation method of PVCL-PVA-PEG/ BBR-MCs described above. HSC-T6 cells were first seeded in 12-well plates at 1×10^5 cells/well and cultured overnight to examine cellular uptake. After 24h, the medium was replaced with DMEM containing free Cou-6 and PVCL-PVA-PEG/Cou6-MCs (equal amounts of Cou-6 200ng/mL), and then the cells were incubated at 37°C for 5min, 0.5h, 1h and 2h. After washing three times with ice-cold PBS to remove free Cou6 or Cou6 micelles that had not been uptaken, the cells were visualized directly with a fluorescence microscope or digested with 0.25% trypsin-EDTA and then collected for detection by flow cytometry.

In vitro Anti Hepatic Stellate Cell Activation Assay of PVCL-PVA -PEG/BBR-MCs

The inhibitory ability of PVCL-PVA-PEG/BBR-MCs on HSC-T6 cell activation and collagen production was investigated by detecting the expression of α-SMA and type I collagen. HSC-T6 cells were seeded in 6-well plates and cultured for 24h. The cells were randomly divided into the following five groups: control group (2% DMEM 25h), TGF-β1 group (2% DMEM 1h + TGF-β1 24h), free group (15 μM free BBR 1 h + TGF-β1 24h), PVCL-PVA-PEG/BBR-MCs group (15 μM PVCL-PVA-PEG/BBR-MCs 1 h + TGF-β1 24h), the blank MCs group (blank MCs 1 h+ TGF-β1 24h). All groups incubated with the preparation for 1 h were then co-cultured for 24 h with 5 ng/mL TGF-β1. After 24h of culture, HSC-T6 cells were extracted for proteins with ice-cold RIPA buffer, and the expression of α-SMA (12% gel) and collagen I (6% gel) was detected by Western blot.[37]

Cell Migration Assay of PVCL-PVA-PEG/BBR-MCs

Cell scratch assay was used to assess the influence of PVCL-PVA-PEG/BBR-MCs on TGF-β1-induced HSC cell migration. HSC-T6 cells were seeded in 6-well plates at a concentration of 5×10^5 cells/well. After the cells were fully grown, a linear wound was induced by scratching the cells with a tip and washed three times. Subsequently, cells were treated with free BBR, PVCL-PVA-PEG/BBR-MCs, and blank MCs for 1h and then co-cultured with 5 ng/mL TGF-β1 for 24 h. Meanwhile, cells cultured in DMEM containing 2% FBS served as the control group and TGF-β1-induced cells served as the model group. Finally, scratches of HSC-T6 cells were imaged at 0 h and 24 h using fluorescence microscope (Olympus, Tokyo, Japan).

Animals and Ethics Statement

C57BL/6N (male, 6 weeks old) mice were purchased from SiPeiFu of Beijing. The use and handling of mice adhered to ethical guidelines outlined in the National Institutes of Health Guide for the Care and Use of Laboratory Animals. All animal experiments were conducted and approved by the Experimental Animal Management Committee under the Ethics Committee

of the Institute of Materia Medica, Chinese Academy of Medical Sciences and Peking Union Medical College (Beijing, China; No. 00003619). Every effort was made to minimize the number of mice used and to alleviate their suffering.

Hemolytic Activity Test

The hemolysis assay was used as previously to detect erythrocyte damage by PVCL-PVA-PEG/BBR-MCs and free BBR. Briefly, mouse blood was centrifuged at 1500 rpm for 10 min, the supernatant was discarded, and the precipitated cells were repeatedly washed with 0.9% NaCl solution until the supernatant was clear and free of blood-red color. The final concentration of erythrocytes was adjusted to 4% (v/v) with 0.9% NaCl. Free BBR, blank MCs and PVCL-PVA-PEG/BBR-MCs were mixed with the erythrocyte suspension and placed at 37°C for 2 h. Hemolysis rate was recorded as 0 and 100% using 0.9% saline or distilled water as negative and positive controls. Subsequently, 1 mL of the above solution was collected and centrifuged at 3000 rpm for 10 minutes and photographed for image capture.

Biodistribution of PVCL-PVA-PEG/DiD-MCs in Mice

In vivo, animal imaging studies were performed to evaluate the biodistribution of PVCL-PVA-PEG/DiD-MCs in fibrotic mice. PVCL-PVA-PEG/DiD-MCs (200 μg/kg) and free DiD (200 μg/kg) were injected into mice through the tail vein, and then the abdomens of depilated mice were imaged at 3h and 6h using the IVIS Spectrum CT in vivo imaging system (Caliper Life Sciences Inc., Mountain View, CA, USA). At 3 h, the major organs (heart, liver, spleen, lungs, and kidneys) of the mice were harvested for imaging. Finally, the images were analyzed for the intensity of the fluorescence.

In vivo Efficacy Study in a CCl_4-Induced Liver Fibrosis Mouse Model

A hepatic fibrosis mouse model was established by intraperitoneal injection of CCl_4 in olive oil (30%, v/v) at a dose of 10 mL/kg body weight three times per week for 4 weeks.[6] C57 mice were randomly divided into 5 groups: (1) healthy group, (2) CCl_4-induced but not administered group, (3) 20 mg/kg free BBR group, (4) 20 mg/kg PVCL-PVA-PEG/BBR-MCs group, (5) blank MCs (Equivalent amount of 20mg/kg BBR) group. In addition, the formulations of each group were administered via the tail vein after 24 h of CCl_4 injection. After 4 weeks of treatment, mice were pathologically analyzed after 48h of the last injection of PVCL-PVA-PEG/BBR-MCs.

Histologic and Immunochemical Analyses

Paraffin-embedded liver tissues were sectioned at 5 μm. Subsequently, hematoxylin-eosin (H&E) staining, Sirius red staining, and Masson staining were used to evaluate hepatic histopathologic changes and collagen deposition. Finally, slides were photographed at 20x or 10x magnification. The underlying cause of hepatic fibrosis is the activation and proliferation of HSCs, so the activation of HSCs and the amount of fibrillar collagen can reflect the degree of hepatic fibrosis. Immunochemical staining was performed as previously reported: to block endogenous peroxidase, liver sections were deparaffinized, rehydrated and incubated with 3% hydrogen peroxide. They were then heated in 10 mM sodium citrate buffer to retrieve the antigen and mounted in 5% BSA solution. Finally, liver sections were sequentially incubated with primary antibodies (α-SMA and collagen I) and secondary antibodies.[38]

Pharmacokinetic Study

Before the experiment, male Sprague-Dawley rats (180–220 g) were acclimatized for one week in an environmentally controlled housing chamber. A fully dissolved and clarified solution of free BBR was prepared using a solvent consisting of 10% DMSO + 40% PEG300 + 5% Tween 80 + 45% NaCl (0.9%). PVCL-PVA-PEG/BBR-MCs were prepared by the film dispersion method as previously described. Free BBR solution (1 mg/mL) and PVCL-PVA-PEG/BBR-MCs (1 mg/mL) were administered intravenously (i.v.) to SD rats at a dose of 10 mg/kg body weight via the tail vein, and the blood was then centrifuged at 5000 rpm for 10 min to obtain plasma. Mix 25 μL of plasma sample with 200 μL of acetonitrile (containing Palmatine internal standard) to precipitate proteins, vortex for 5 minutes, then centrifuge at 4000 rpm for 10 minutes at 4°C and analyze the supernatant by LC-MS/MS.[39] The blood samples were analyzed using the following chromatographic conditions as described below: the mobile phases were 0.1% formic acid in water (A) and 0.1% formic acid in acetonitrile (B) with the following program profile 0–0. 5 min, A (90%) vs B (10%), 0.5–4.0 min, A (90%~5%) vs B (10%~95%), 4.0–6.0

min, A (5%) vs B (95%), 6.0–6.1 min, A (5%~90%) vs B (95%~10%), 6.1–9.0 min, A (90%) vs B (10%). The mobile phase was pumped at a flow rate of 0.3 mL/min and the column temperature was 25 °C. Winnonlin software was used to calculate various pharmacokinetic parameters.

In vivo Safety Assay of PVCL-PVA-PEG/BBR-MCs

C57BL/6 mice were randomized into three groups (n = 3): saline, free BBR, and PVCL-PVA-PEG/BBR-MCs (equal amounts of BBR 20 mg/kg). Each group of preparations was injected into the tail vein of the mice once every other day. Mice were sacrificed after 4 weeks of treatment. The heart, liver, spleen, lungs, and kidneys were excised after abdominal disinfection, and histological analysis (H&E staining) was performed to evaluate the in vivo biosafety of PVCL-PVA-PEG/BBR-MCs.

Statistical Analysis

Results represent mean ± standard deviation (SD). Student's *t*-test was performed to compare between the two groups. A value of P less than 0.05 was considered statistically significant.

Results and Discussion

Preparation and Characterization of PVCL-PVA-PEG/BBR-MCs

The schematic structure of PVCL-PVA-PEG/BBR-MCs is shown in the Schematic illustration. The mass ratio of BBR and PVCL-PVA-PEG was identified by size, PDI, EE%, and DL% of PVCL-PVA-PEG/BBR-MCs. Figure 1A shows the particle size and PDI, and the results indicate that all the formulations have a particle size of less than 100 nm and a PDI of less than 0.15. The zeta potential (Figure 1B) of all micelles exhibits a positive surface charge. Notably, mass ratios 1/15 and 1/18 have lower size and PDI than the others. In addition, Figure 1C suggested that higher EE% for mass ratios 1/15 and 1/18 than the others. However, the micelles with a mass ratio of 1/15 exhibited a higher LC% than the micelles with a mass ratio of 1/18. Therefore, the mass ratio of 1/15 (BBR: PVCL-PVA-PEG) was chosen as the final prescription for the preparation of PVCL-PVA-PEG/BBR-MCs. In conclusion, the final formulation of PVCL-PVA-PEG/BBR-MC was 98.52% ± 0.70 for EE% and 6.16% ± 0.04 for LD%.

The average particle size of the prepared PVCL-PVA-PEG/BBR-MCs was about 60.04 ± 0.027 nm with a positive surface charge of 1.49 ± 0.32 mV (Figure 1D and E). Figure 1F shows that PVCL-PVA-PEG /BBR-MCs had a yellow, clear and transparent appearance, indicating that the preparation of BBR into micelles greatly improved its solubility in water. TEM results suggested that the morphology of PVCL-PVA-PEG/BBR-MCs was homogeneously dispersed and in a shape of spherical, and its diameter was consistent with the DLS results (Figure 1G). To further validate the stability of the formulations, the particle size stability of PVCL-PVA-PEG/BBR-MCs was investigated over two weeks using DLS. As illustrated in Figure 1H, the PVCL-PVA-PEG/BBR-MCs exhibited remarkable stability. Finally, the successful encapsulation of BBR into the micellar core by PVCL-PVA-PEG was confirmed using FTIR. Figure 1I demonstrates that PVCL-PVA-PEG/BBR-MCs exhibit the distinctive C-H stretching vibrational absorption peak of PVCL-PVA-PEG at 2900 cm-1, indicating that BBR was entirely encapsulated within the micelle.

Vitro Cell Viabilities of BBR and PVCL-PVA-PEG/BBR-MCs

CCK-8 assay was used to estimate the viability of free BBR, blank MCs, and PVCL-PVA-PEG/BBR-MCs to quiescent HSC-T6 cells. As shown in Figure 2A, the cell viability of HSC-T6 cells treated with blank MCs was above 90% at concentrations ranging from 0.9375–120 μM, which suggested that the blank micelles showed excellent biocompatibility.

Subsequently, we investigated the effects of free BBR and PVCL-PVA-PEG/BBR-MCs on the viability of quiescent HSC-T6 cells. Figure 2B shows that there was no significant cytotoxicity of free BBR against HSC-T6 in the range of 0.9375–120 μM. Similarly, the cellular activities of PVCL-PVA-PEG/BBR-MCs on HSC-T6 cells were all greater than 90% at concentrations in the range of 0.9375–30 μM, indicating that PVCL-PVA-PEG/BBR-MCs did not have a toxic effect on normal HSC-T6 cells (Figure 2C). However, cell viability was below 80% at concentrations of 60–120 μM, indicating that PVCL-PVA-PEG/BBR-MCs produced significant cytotoxicity against HSC-T6, which may be attributed to the fact that the PVCL-PVA-PEG carrier increased BBR entry into the cells, with excessive concentrations leading to cell death.

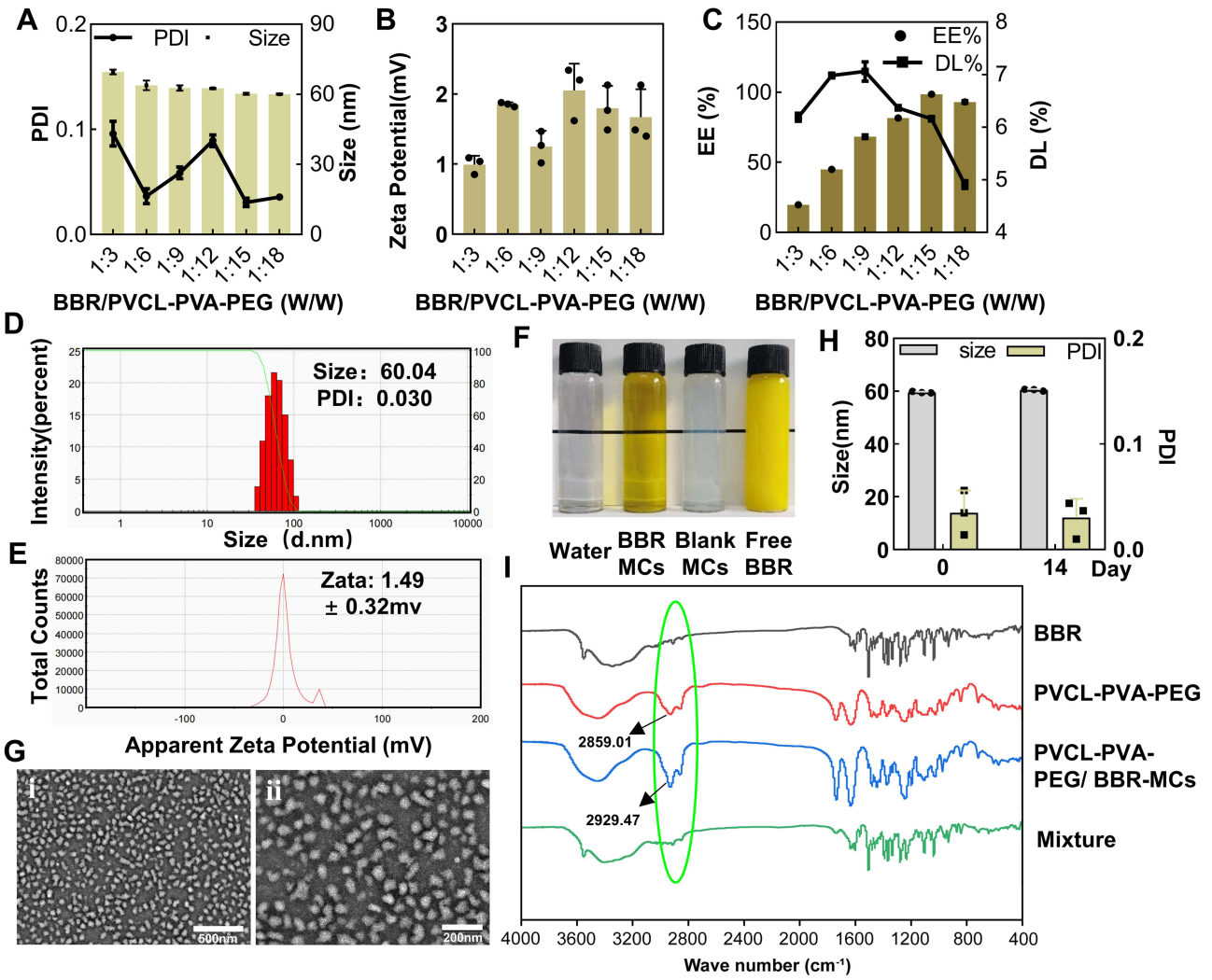

Figure 1 Optimization and characterization of PVCL-PVA-PEG/BBR-MCs formulation. (**A–C**) Optimization of PVCL-PVA-PEG/BBR-MCs formulation (n=3). (**D** and **E**) Particle size and potential of PVCL-PVA-PEG/BBR-MCs. (**F**) Appearance of PVCL-PVA-PEG/BBR-MCs. (**G**) TEM image of PVCL-PVA-PEG/BBR-MCs; scale bars are 500nm (i) and 200 nm (ii). (**H**) Size stability of PVCL-PVA-PEG/BBR-MCs over two weeks. (**I**) FTIR images of BBR, PVCL-PVA-PEG, PVCL-PVA-PEG/BBR-MCs, and the mixture of BBR and PVCL-PVA-PEG.

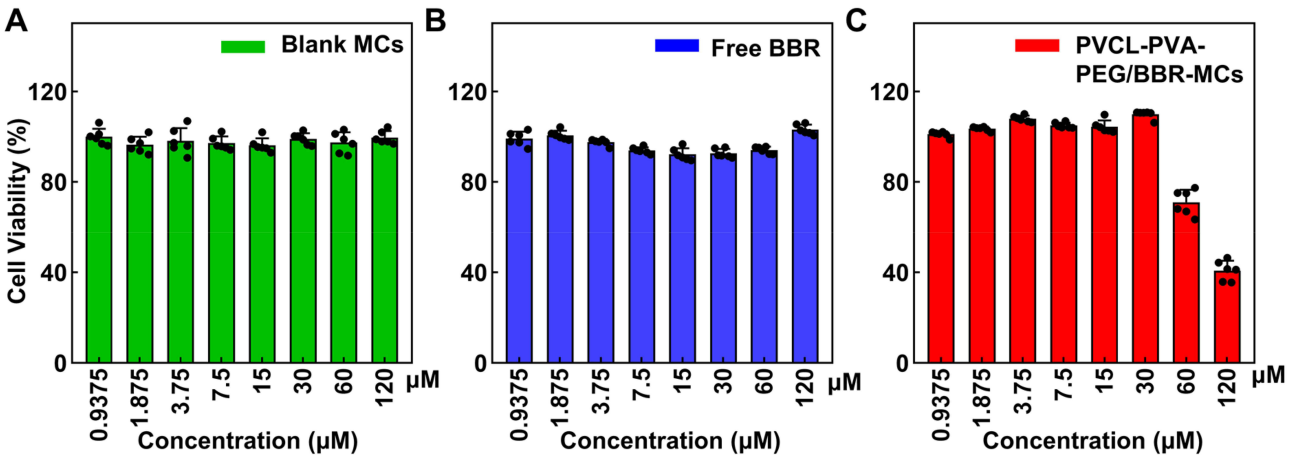

Figure 2 Cytotoxicity assays. Cytotoxicity of blank micelles (**A**), free BBR (**B**), and PVCL-PVA-PEG/Cou6-MCs (**C**) on HSC-T6 cells (n=6).

PVCL-PVA-PEG/Cou6-MCs Improve the Cellular Uptake of HSC-T6 Cells

The uptake capacity and fate of PVCL-PVA-PEG/Cou6-MCs by HSC-T6 cells were determined by fluorescence microscopy and flow cytometry. Figure 3A and B show fluorescence images of free Cou6 and PVCL-PVA-PEG/Cou6-MCs taken up by HSC-T6 cells. The results show that the fluorescence intensity of PVCL-PVA-PEG/Cou6-MCs was stronger than that of free Cou6 for the same period. In addition, the fluorescence intensity of the PVCL-PVA-PEG/Cou6-MCs showed a time-dependent enhancement at 30 min with the extension of time. The fluorescence intensity at 1 and 2 hours was similar to that at 30 minutes, suggesting that the uptake of PVCL-PVA-PEG/Cou6-MCs by HSC-T6 cells is maximal from 30 minutes to 1 h. Figure 3C shows the analysis of the fluorescence intensity of the fluorescence microscope images. Subsequently, the uptake of free Cou6 and PVCL-PVA-PEG/Cou6-MCs by HSC-T6 cells at 5 min, 30 min and 1 h was determined by flow cytometry. Flow cytometry results showed that the uptake of free Cou6 and PVCL-PVA-PEG/Cou6-MCs increased over time at 1 hour (Figure 3D and E).

Inhibition of the Activation of HSC-T6 Cells and the Formation of Collagen by PVCL-PVA-PEG/BBR-MCs

The activation of hepatic stellate cells, followed by the secretion of excess extracellular matrix, is a key link in the progression of liver fibrosis.[40,41] α-SMA is an important marker of hepatic stellate cells and represents the degree of

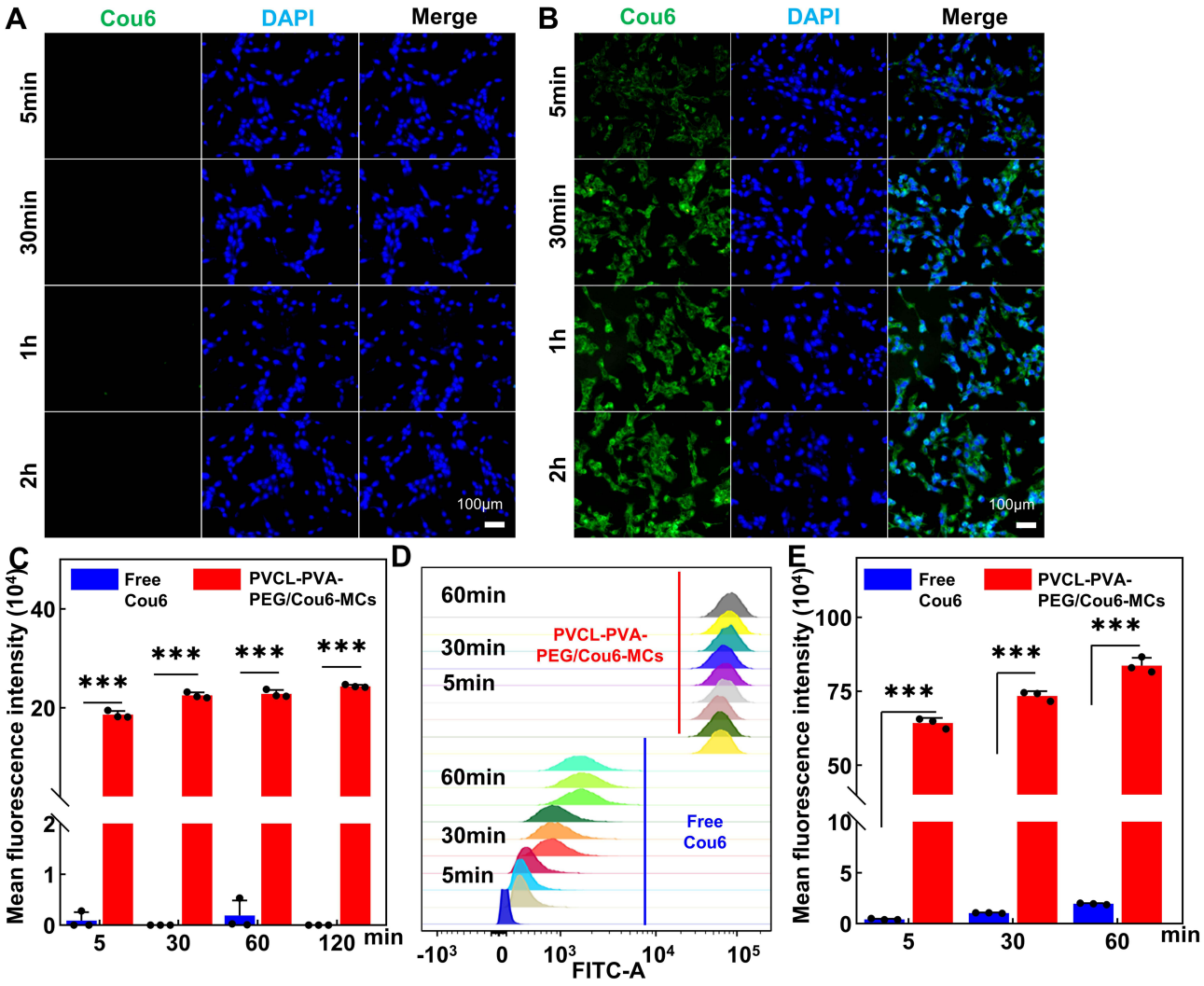

Figure 3 Cellular uptake assay of Cou6-loaded PVCL-PVA-PEG micelles. (**A** and **B**) Fluorescence microscopy detection images of HSC-T6 cells against free Cou6 (**A**) and PVCL-PVA-PEG/Cou6-MCs (**B**) at 5 min, 30 min, 1 h and 2 h (n=3). (**C**) Quantitative analysis of fluorescence microscopy images (n=3). (**D**) Flow cytometric results of HSC-T6 cells against free Cou6 and PVCL-PVA-PEG/Cou6-MCs at 5 min, 30 min, and 1 h (n=3). (**E**) Flow cytometric analysis of free Cou6 and PVCL-PVA-PEG/Cou6-MCs (n=3). Data represented as mean ± SD, n = 3; ***p < 0.001.

activation of hepatic stellate cells.[8,42] Collagen I is an important collagen component of the extracellular matrix and represents the degree of fibrosis.[8,43] To investigate the effects of PVCL-PVA-PEG/BBR-MCs on HSC-T6 activation and inhibition of collagen production, we examined the expression of α-SMA and collagen I in HSC-T6 cells by Western blot. The results (Figure 4A and B) showed that the expression of α-SMA and collagen I was increased in HSC-T6 cells in the TGF-β1 (5 ng/mL) group, which was significantly higher than that in DMEM-treated cells ($P<0.05$). The blank micelle group did not have any effect on the expression of α-SMA and collagen I in the activated HSC-T6. Furthermore, TGF-β1 (5 ng/mL)-activated HSCs treated with free BBR showed decreased α-SMA expression compared to the model group (Figure 4A and C). It was further found that the PVCL-PVA-PEG/BBR-MCs group expressed less α-SMA than the model group ($P<0.05$) and the free BBR group ($P<0.01$) (Figure 4A and C). The results of collagen I (Figure 4B and D) showed that the collagen I expression in the free BBR-treated group was lower than that in the TGF-β1-treated group ($P<0.05$). Most importantly, collagen I expression was lowest in the PVCL-PVA-PEG/BBR-MCs group in comparison to the TGF-β1 group ($P<0.01$) and the free BBR group ($P<0.01$). These results are consistent with cell uptake results, suggesting that PVCL-PVA-PEG encapsulated micelles of BBR may enhance cell uptake and thus therapeutic efficacy of BBRs.

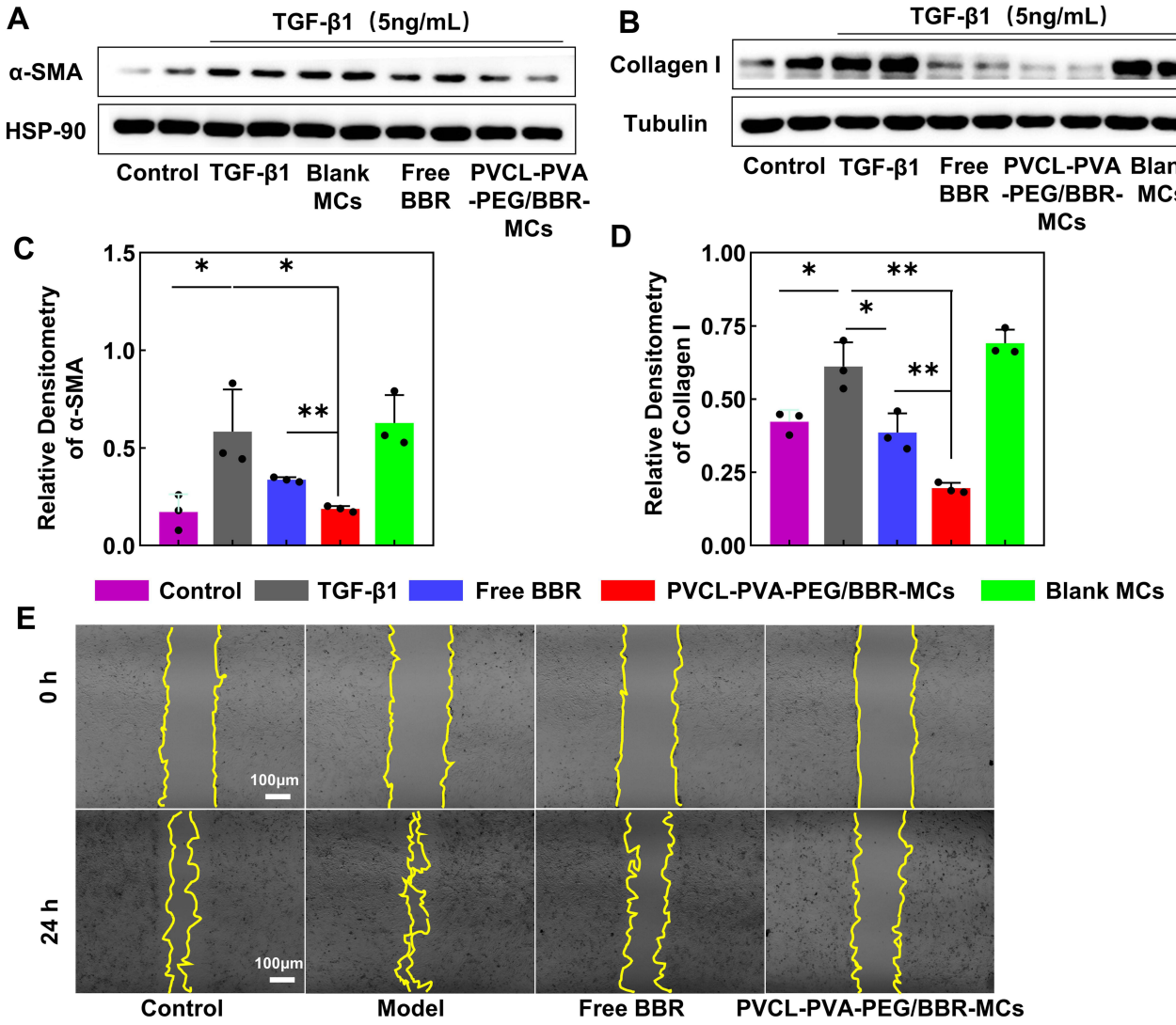

Figure 4 In vitro antifibrosis experiments of PVCL-PVA-PEG/BBR-MCs. (**A** and **B**) Protein expression of α-SMA (**A**) and collagen I (**B**) in HSC-T6 cells treated with PVCL-PVA-PEG/BBR-MCs (n=3). (**C** and **D**) Quantitative analysis of protein expression of α-SMA (**C**) and collagen I (**D**) (n=3). (**E**) Changes in the migration of HSC-T6 cells treated with PVCL-PVA-PEG/BBR-MCs (n = 3). Data represented as mean ± SD, n = 3; *p < 0.05, **p < 0.01.

BBR Inhibited TGF-β1-Induced Migration of HSC-T6 Cells

For the progression of liver fibrosis, activated HSCs with highly migratory properties are essential. A cell scratch assay was used to evaluate changes in the migratory properties of activated HSC-T6 cells after drug treatment. The healing of the cell scratches was imaged at 0 h and 24 h after the drug treatment. From Figure 4E, it can be seen that the cells without any treatment showed a tendency to heal within 24 hours, which indicates that the cells have proliferative and migratory properties. In addition, TGF-β1-treated wounds healed significantly within 24 hours compared with control, suggesting that activated HSCs have stronger migratory properties. It was further observed that the cell scratches in the group treated with free BBR healed more slowly at 24 hours than at 0 hours, and the width of the scratches was larger than that in the model group, demonstrating that BBR inhibited the migration of HSC-T6 cells. Most importantly, after 24 hours of treatment with PVCL-PVA-PEG/BBR-MCs, the scratches were the widest when compared to the model and free groups, suggesting that PVCL-PVA-PEG/BBR-MCs promote more BBR into the cells. Overall, the scratch assay suggested that PVCL-PVA-PEG/BBR-MCs could inhibit the migration and proliferation of activated HSC-T6 cells.

Local Delivery of PVCL-PVA-PEG/BBR-MCs to Hepatic Fibrosis

Taking into account the efficient uptake of PVCL-PVA-PEG/Cou6-MCs by HSC-T6 cells in vitro (Figure 3), we assessed the biodistribution of PVCL-PVA-PEG/DiD-MCs and free DiD (200 μg/mL) in fibrotic mice using both in vivo animal imaging and ex vivo imaging of organs. Figure 5A revealed that at 3h and 6h, the abdomens of mice of the PVCL-PVA-PEG/DiD-MCs group exhibited stronger fluorescence than the free DiD group (Figure 5B, $P < 0.01$). Subsequently, 3 h after injection, the animals were sacrificed and major organs were removed, which revealed that the PVCL-PVA-PEG/DiD-MCs group was predominantly located in the liver, spleen, and lungs, and free DiD was predominantly located in the liver and spleen (Figure 5C). Furthermore, it was noticed that the PVCL-PVA-PEG/DiD-MCs group showed the strongest

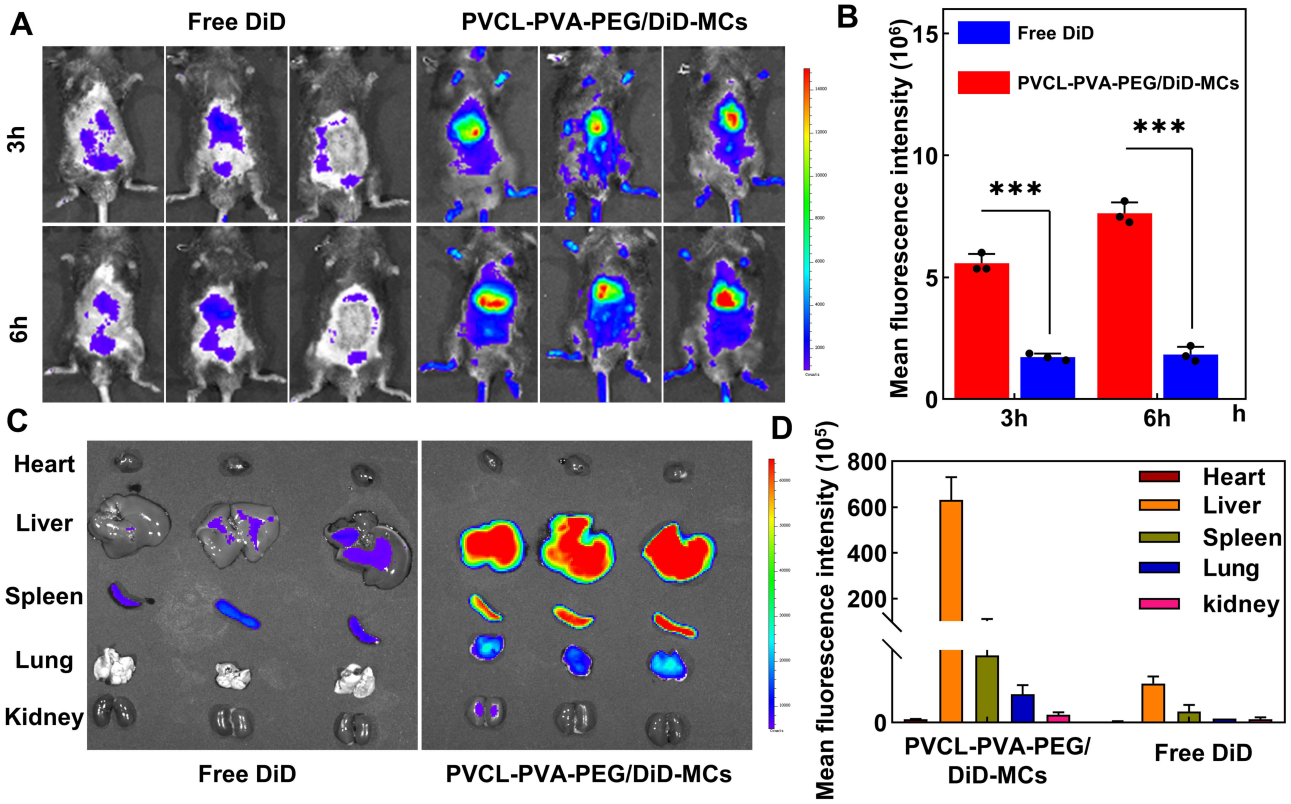

Figure 5 In vivo biodistribution studies of PVCL-PVA-PEG/DiD-MCs. (**A**) In vivo imaging in mice after injection of free DiD and PVCL-PVA-PEG/DiD-MCs for 3h and 6h. (**B**) Quantification of fluorescence intensity at 3 h and 6 h after injection of free DiD and PVCL-PVA-PEG/DiD-MCs into mice (n = 3). (**C**) Ex vivo imaging of stripped organs in mice 3 hours after injection of free DiD and PVCL-PVA-PEG/DiD-MCs (n=3). (**D**) Quantification of fluorescence intensity in mouse liver 3 h after injection of free DiD and PVCL-PVA-PEG/DiD-MCs. Data represented as mean ± SD, n = 3; ***p < 0.001.

fluorescence intensity of the liver (Figure 5D). The above findings suggest that PVCL-PVA-PEG/DiD-MCs have a greater ability to enter the liver for two possible reasons: 1) PVCL-PVA-PEG increased the solubility of free DiD, allowing DiD to be dispersed in the blood with smaller particle size and then transported to the liver; and 2) the encapsulation of PVCL-PVA-PEG exerted a protective effect on free DiD, which reduced the degradation action of blood on DiD.

PVCL-PVA-PEG/BBR-MCs Alleviate CCl_4-Induced Liver Fibrosis and HSCs Activation

Based on the inhibition of HSCs activation (Figure 4A) and the reduction of collagen levels (Figure 4B) by PVCL-PVA-PEG/BBR-MCs in vitro, the anti-fibrogenic effects of PVCL-PVA-PEG/BBR-MCs were evaluated in a CCl_4-induced mouse model. The in vivo antifibrotic effects of PVCL-PVA-PEG/BBR-MCs were evaluated by H&E staining, Sirius red staining, and Masson's staining. H&E staining revealed that CCl_4-induced mouse liver sections showed signs of inflammation, including adjacent portal edema, neutrophilic infiltration, and disseminated hepatocellular necrosis (Figure 6A). In addition, it was found that the effect of free BBR on the inflammation of the liver was very weak. However, the PVCL-PVA-PEG/BBR-MCs significantly alleviated the signs of inflammatory cell

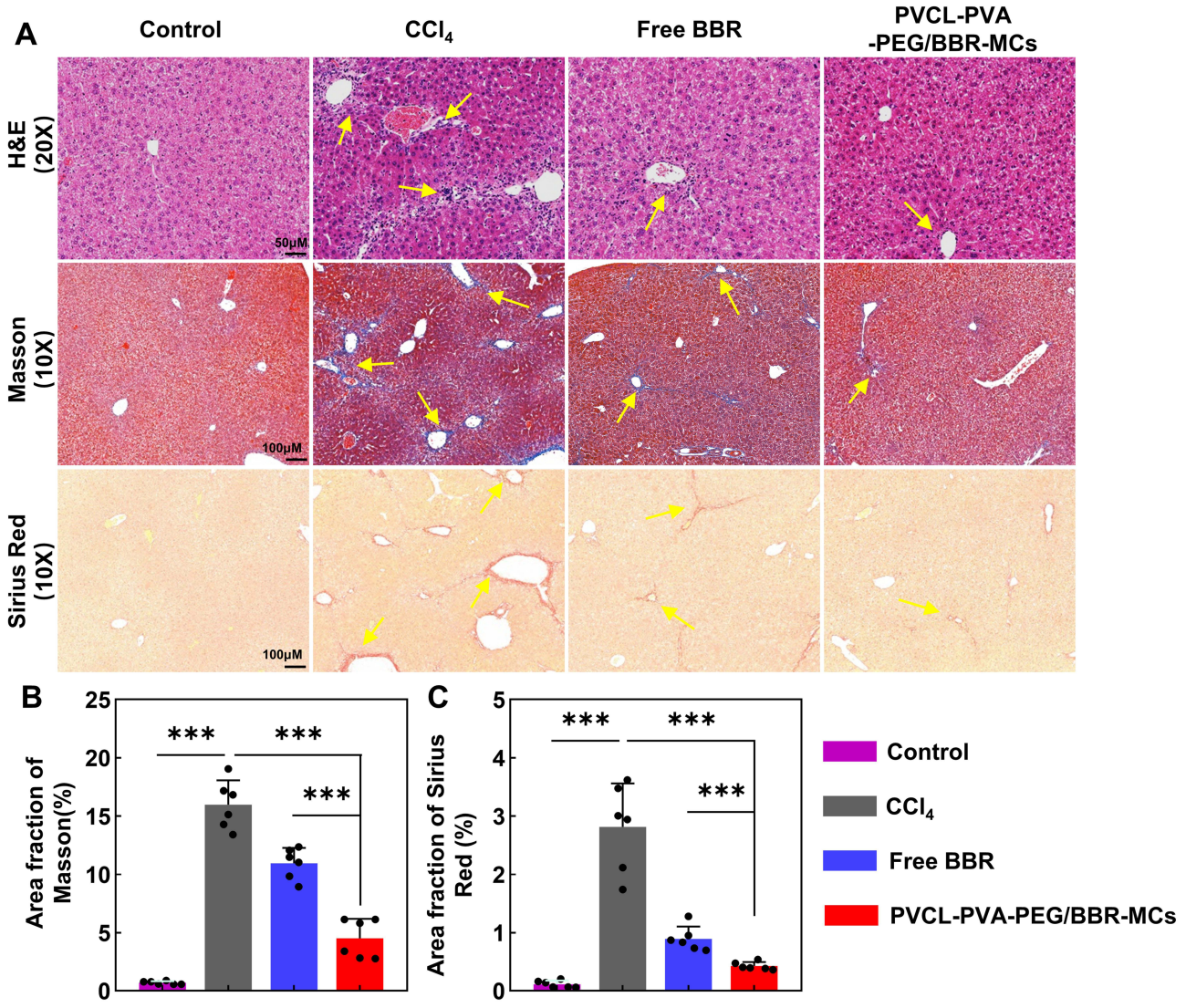

Figure 6 PVCL-PVA-PEG/BBR-MCs attenuate the progression of hepatic fibrosis in CCl4-induced mice. (**A**) Representative images of liver sections stained with H&E, Masson, and Sirius Red from CCl4-induced mice treated with BBR formulations; scale bars are 50 μm (20 ×) and 100 μm (10 ×). (**B** and **C**) Quantitative analysis of liver slides of (**B**) Masson and (**C**) Sirius red. Data represented as mean ± SD, n = 6; ***p < 0.001. The yellow arrows show changes in inflammation and collagen after treatment with free BBR and PVCL-PVA-PEG/BBR-MCs compared with the CCl_4 group.

infiltration and tissue necrosis in comparison with the free BBR group (Figure 6B and C). Furthermore, Sirius Red and Masson staining showed CCl_4 triggered collagen deposition (Figure 6A). It is noteworthy that the collagen accumulation was significantly reduced in the PVCL-PVA-PEG/BBR-MCs treated group of mice, whereas the collagen deposition was slightly improved in the free BBR treated mice (Figure 6B and C). The above results suggest that PVCL-PVA-PEG/BBR-MCs can deliver more BBR drugs to the liver to play a role in the treatment of liver fibrosis.

To further verify whether the administration of PVCL-PVA-PEG/BBR-MCs to the liver exerted further inhibitory effects on the activation of hepatic stellate cells, we used immunohistochemical experiments to examine the levels of α-SMA and collagen I in the liver. Figure 7A showed that CCl_4-induced liver tissues of mice had significantly increased expression of α-SMA and collagen I, suggesting that CCl_4 led to activation of HSCs and increased secretion of extracellular matrix. Interestingly, the liver tissues treated with PVCL-PVA-PEG/BBR-MCs showed a significant reduction in α-SMA and collagen I, whereas the collagen deposition was slightly improved in the group

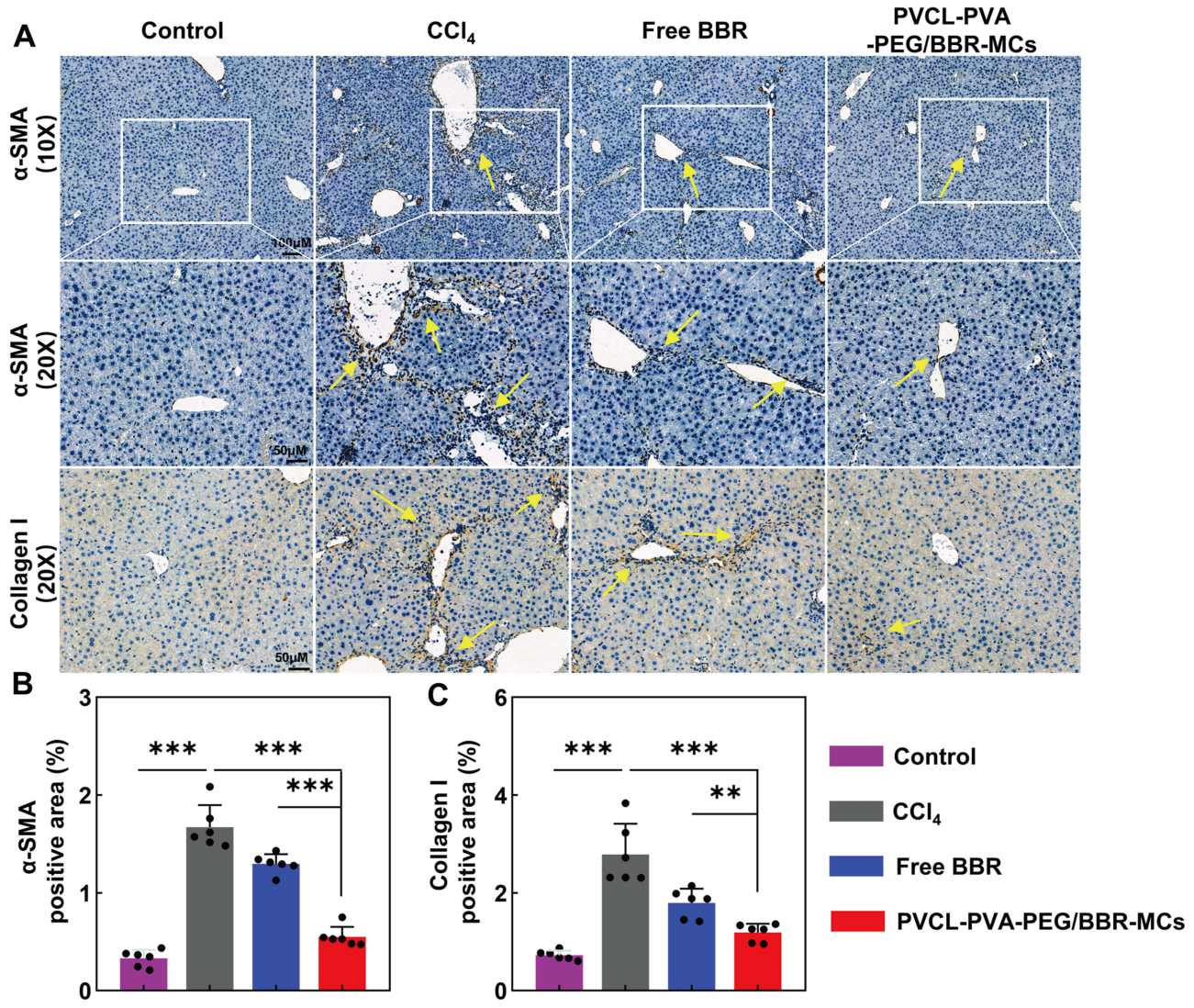

Figure 7 PVCL-PVA-PEG/BBR-MCs inhibit the activation of HSCs in CCl4-induced mice. (**A** and **B**) Representative immunohistochemical staining images and quantitative analysis of α-SMA from liver sections; scale bars are 100 μm (10 ×) and 50 μm (20 ×). (**A** and **C**) Representative immunohistochemical staining images and quantitative analysis of collagen I from liver sections; scale bars are 50 μm (20 ×). Data represented as mean ± SD, n = 6; **p < 0.01, ***p < 0.001. The yellow arrows show changes in α-SMA and collagen I levels after treatment with free BBR and PVCL-PVA-PEG/BBR-MCs compared with the CCl_4 group.

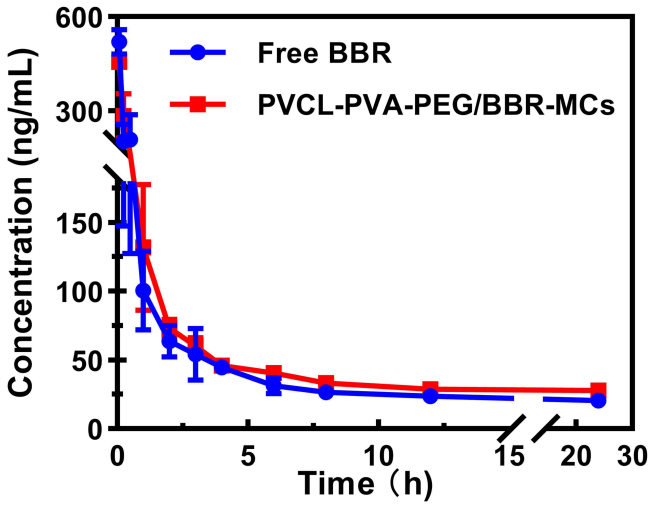

Figure 8 The plasma concentration-time curve of BBR in rats following intravenous administration of a free BBR solution and PVCL-PVA-PEG/BBR-MCs (10 mg/kg) is presented. The data represent the mean ± SD, with three rats per group.

treated with free BBR (Figure 7A–C). The above results suggest that PVA-PEG/BBR-MCs may inhibit the activation of HSCs and the secretion of extracellular matrix, which in turn may suppress the progression of liver fibrosis.

Pharmacokinetics of BBR Formulations After Intravenous Injection

Figure 8 shows the concentration versus time curves for the two BBR formulations. Different from other studies, the free BBR solution group in this study was completely and fully dissolved using the solvent 10% DMSO + 40% PEG300 + 5% Tween 80 + 45% NaCl (0.9%) to obtain a completely clear and transparent BBR solution. Therefore, the free BBR solutions had a longer plasma circulation time after single-dose injection compared to the conventional BBR solution group (formulated with 5% glucose) evaluated by Wang et al.[44] Interestingly, the PVCL-PVA-PEG/BBR-MCs also had a longer haemocirculation time than Wang's. The experimental results showed that the plasma concentration-time curves of free BBR solution and BBR nanomicelles followed the same trend. However, there was a significant difference between them in terms of pharmacokinetic parameters. Table 1 shows the mean pharmacokinetic parameters of the two formulations, which showed that PVCL-PVA-PEG/BBR-MCs had higher area under the curve (AUC) and lower rate of clearance (CL) values than the free BBR solution prepared in this study, indicating that PVCL-PVA-PEG/BBR-MCs have longer plasma circulation time and higher drug exposure in vivo. The above phenomenon implies that although the plasma concentration-time curves of free BBR solution and PVCL-PVA-PEG/BBR-MCs showed similar trends, PVCL-PVA-PEG/BBR-MCs showed significant advantages in pharmacokinetic parameters. To a certain extent, PVCL-PVA-PEG may have improved the stability and bioavailability of BBR in vivo, reduced the rate of blood clearance, prolonged the elimination half-life and the mean residence time, and

Table 1 Pharmacokinetic Parameters of BBR in Rats After Intravenous Administration. (10 Mg/Kg, mean±SD, n = 3)

Parameter	Unit	Free BBR Solution	PVCL-PVA-PEG/BBR-MCs
$t_{1/2}$[a]	h	18.25 ± 3.04	23.48 ± 5.07
AUC $_{(0-24)}$[b]	h*ng/mL	932.92 ± 75.88	1089.42 ± 48.12
AUC $_{(0-\infty)}$	h*ng/mL	1400.59 ± 26.39	1924.09 ± 283.53
MRT $_{(0-t)}$[c]	h	7.43 ± 0.39	8.07 ± 0.16
MRT $_{(0-\infty)}$	h	21.89 ± 4.39	29.68 ± 6.50
CL[d]	mL/h/kg	6818.59 ± 139.36	4965.32 ± 671.34

Notes: [a]Half-life. [b]Area under the plasma concentration-time curve. [c]Mean retention time. [d]Rate of clearance.

prolonged the exposure time of the drug. The free BBR solution in this experiment showed a longer plasma circulation time due to complete solubilization compared to the study by Wang et al. However, PVCL-PVA-PEG/BBR-MCs showed more improved AUC values and longer circulation times under the same conditions, further validating the potential of PVCL-PVA-PEG to improve drug stability and prolong circulation time in vivo.

PVCL-PVA-PEG/BBR-MCs Have High Safety

The influence of free BBR, PVCL-PVA-PEG/BBR-MCs on the major organs of healthy mice was evaluated using H&E staining. Compared with the saline group, free BBR did not cause any damage to the heart, liver, spleen, lungs, or kidneys. In addition, PVCL-PVA-PEG/BBR-MCs were not found to be significantly toxic to major organ tissues (Figure S1).

The hemolytic assay was used to determine whether PVCL-PVA-PEG/BBR-MCs (5 mg/mL) and a 10-fold dilution of the formulations had a hemolytic effect on blood cells. It was found that there was no significant hemolysis of PVCL-PVA-PEG/BBR-MCs even at high concentrations (5 mg/mL), suggesting that PVCL-PVA-PEG/BBR-MCs have good hemocompatibility (Figure S2). In summary, PVCL-PVA-PEG can be used as a safe carrier for drug delivery to the liver.

Conclusion

We prepared biocompatible BBR-loaded micelles (PVCL-PVA-PEG/BBR-MCs) using the amphiphilic material PVCL-PVA-PEG as a carrier. The DLS showed that the PVCL-PVA-PEG/BBR-MCs had a homogeneous particle size and a slightly positive potential. PVCL-PVA-PEG/BBR-MCs were taken up by HSC-T6 cells to a greater extent than free BBR. In vitro studies showed that PVCL-PVA-PEG/BBR-MCs significantly reduced the expression of α-SMA and collagen I, and inhibited the migration of activated HSC-T6 cells. In vivo, biodistribution experiments showed that the self-assembled PVCL-PVA-PEG micelles were able to actively accumulate in the liver. In vivo efficacy studies showed that PVCL-PVA-PEG/BBR-MCs significantly reduced the infiltration of inflammatory cells, decreased the deposition of collagen and inhibited the activation of HSCs. The safety evaluation showed excellent biocompatibility of the PVCL-PVA-PEG/BBR-MCs. In conclusion, PVCL-PVA-PEG/BBR-MCs have great potential as biocompatible micellar systems for liver delivery of hydrophobic anti-hepatic fibrosis drugs.

Acknowledgments

Xiaozhu Zha and Yumei Hao are co-first authors for this study. This study was supported by Key Project Foundation of Natural Science Research in Universities of Anhui Province (No. 2023AH053428 and No. KJ2021A0300), Yunnan Key Laboratory of Southern Medicinal Utilization, Yunnan University of Chinese Medicine (202105AG070012XS2249) and the mixed curriculum fund of Anqing Medical College (No.2019HK013 and No. 2021HK006).

Author Contributions

All authors made a significant contribution to the work reported, whether that is in the conception, study design, execution, acquisition of data, analysis and interpretation, or in all these areas; took part in drafting, revising or critically reviewing the article; gave final approval of the version to be published; have agreed on the journal to which the article has been submitted; and agree to be accountable for all aspects of the work.

Disclosure

The authors report no conflicts of interest in this work.

References

1. Koyama Y, Brenner DA. Liver inflammation and fibrosis. *J Clin Invest*. 2017;127(1):55–64. doi:10.1172/JCI88881
2. Liu X, Tan S, Liu H, et al. Hepatocyte-derived MASP1-enriched small extracellular vesicles activate HSCs to promote liver fibrosis. *Hepatology*. 2023;77(4):1181–1197. doi:10.1002/hep.32662
3. Rosenberg WM. Rating fibrosis progression in chronic liver diseases. *J Hepatol*. 2003;38(3):357–360. doi:10.1016/S0168-8278(03)00010-2

4. Cai J, Hu M, Chen Z, et al. The roles and mechanisms of hypoxia in liver fibrosis. *J Transl Med*. 2021;19(1):186. doi:10.1186/s12967-021-02854-x
5. Li F, Zhao Y, Cheng Z, et al. Restoration of sinusoid fenestrae followed by targeted nanoassembly delivery of an anti-fibrotic agent improves treatment efficacy in liver fibrosis. *Adv Mater*. 2023;35(17):2212206.
6. Zhou L, Liang Q, Li Y, et al. Collagenase-I decorated co-delivery micelles potentiate extracellular matrix degradation and hepatic stellate cell targeting for liver fibrosis therapy. *Acta Biomater*. 2022;152:235–254. doi:10.1016/j.actbio.2022.08.065
7. Qiao JB, Fan -Q-Q, Xing L, et al. Vitamin A-decorated biocompatible micelles for chemogene therapy of liver fibrosis. *J Control Release*. 2018;283:113–125. doi:10.1016/j.jconrel.2018.05.032
8. Zhou Q, Rong C, Gu T, et al. Mesenchymal stem cells improve liver fibrosis and protect hepatocytes by promoting microRNA-148a-5p-mediated inhibition of Notch signaling pathway. *Stem Cell Res Ther*. 2022;13(1):354. doi:10.1186/s13287-022-03030-8
9. Bates J, Vijayakumar A, Ghoshal S, et al. Acetyl-CoA carboxylase inhibition disrupts metabolic reprogramming during hepatic stellate cell activation. *J Hepatol*. 2020;73(4):896–905. doi:10.1016/j.jhep.2020.04.037
10. Sun WY, Gu Y-J, Li X-R, et al. beta-arrestin2 deficiency protects against hepatic fibrosis in mice and prevents synthesis of extracellular matrix. *Cell Death Dis*. 2020;11(5):389. doi:10.1038/s41419-020-2596-8
11. Bansal R, Prakash J, Post E, et al. Novel engineered targeted interferon-gamma blocks hepatic fibrogenesis in mice. *Hepatology*. 2011;54(2):586–596. doi:10.1002/hep.24395
12. Sun Y, Zhou J, Wu X, et al. Quantitative assessment of liver fibrosis (qFibrosis) reveals precise outcomes in Ishak ”stable” patients on anti-HBV therapy. *Sci Rep*. 2018;8(1):2989. doi:10.1038/s41598-018-21179-2
13. Cho JJ, Hocher B, Herbst H, et al. An oral endothelin-A receptor antagonist blocks collagen synthesis and deposition in advanced rat liver fibrosis. *Gastroenterology*. 2000;118(6):1169–1178. doi:10.1016/S0016-5085(00)70370-2
14. Owen T, Carpino G, Chen L, et al. Endothelin receptor-a inhibition decreases ductular reaction, liver fibrosis, and angiogenesis in a model of cholangitis. *Cell Mol Gastroenterol Hepatol*. 2023;16:513–540. doi:10.1016/j.jcmgh.2023.06.005
15. Morgan TR, Weiss DG, Nemchausky B, et al. Colchicine treatment of alcoholic cirrhosis: a randomized, placebo-controlled clinical trial of patient survival. *Gastroenterology*. 2005;128(4):882–890. doi:10.1053/j.gastro.2005.01.057
16. Sokar SS, El-Sayad ME-S, Ghoneim ME-S, et al. Combination of Sitagliptin and Silymarin ameliorates liver fibrosis induced by carbon tetrachloride in rats. *Biomed Pharmacother*. 2017;89:98–107. doi:10.1016/j.biopha.2017.02.010
17. Zhu C, Li K, Peng -X-X, et al. Berberine a traditional Chinese drug repurposing: its actions in inflammation-associated ulcerative colitis and cancer therapy. *Front Immunol*. 2022;13:1083788. doi:10.3389/fimmu.2022.1083788
18. Imenshahidi M, Hosseinzadeh H. Berberis Vulgaris and Berberine: an Update Review. *Phytother Res*. 2016;30(11):1745–1764. doi:10.1002/ptr.5693
19. Wei W, Zeng Q, Wang Y, et al. Discovery and identification of EIF2AK2 as a direct key target of berberine for anti-inflammatory effects. *Acta Pharm Sin B*. 2023;13(5):2138–2151. doi:10.1016/j.apsb.2022.12.009
20. Hashemzaei M, Rezaee R. A review on pain-relieving activity of berberine. *Phytother Res*. 2021;35(6):2846–2853. doi:10.1002/ptr.6984
21. Li C, Leng Q, Li L, et al. Berberine ameliorates obesity by inducing GDF15 secretion by brown adipocytes. *Endocrinology*. 2023;164(4). doi:10.1210/endocr/bqad035
22. Wang N, Xu Q, Tan HY, et al. Berberine inhibition of fibrogenesis in a rat model of liver fibrosis and in hepatic stellate cells. *Evid Based Complement Alternat Med*. 2016;2016:8762345. doi:10.1155/2016/8762345
23. Yi J, Wu S, Tan S, et al. Berberine alleviates liver fibrosis through inducing ferrous redox to activate ROS-mediated hepatic stellate cells ferroptosis. *Cell Death Discov*. 2021;7(1):374. doi:10.1038/s41420-021-00768-7
24. Yang Z, Bian M, Ma J, et al. Berberine regulates pulmonary inflammatory microenvironment and decreases collagen deposition in response to bleomycin-induced pulmonary fibrosis in mice. *Basic Clin Pharmacol Toxicol*. 2023;132(2):154–170. doi:10.1111/bcpt.13818
25. Ahmedy OA, El-Tanbouly DM, Al-Mokaddem AK, et al. Insights into the role of P2X7R/DUSP6/ERK1/2 and SIRT2/MDM2 signaling in the nephroprotective effect of berberine against cisplatin-induced renal fibrosis in rats. *Life Sci*. 2022;309:121040. doi:10.1016/j.lfs.2022.121040
26. Wang FM, Yang Y-J, Ma -L-L, et al. Berberine ameliorates renal interstitial fibrosis induced by unilateral ureteral obstruction in rats. *Nephrology*. 2014;19(9):542–551. doi:10.1111/nep.12271
27. Li G, Dong L, Gao F. GW28-e0988 Berberine attenuates cardiac fibrosis via downregulating IGF1R in diabetic rats. *J Am Coll Cardiol*. 2017;70(16):C38. doi:10.1016/j.jacc.2017.07.131
28. Wang Y, Liao J, Luo Y, et al. Berberine alleviates doxorubicin-induced myocardial injury and fibrosis by eliminating oxidative stress and mitochondrial damage via promoting Nrf-2 pathway activation. *Int J Mol Sci*. 2023;24(4):3257.
29. Khoshandam A, Imenshahidi M, Hosseinzadeh H. Pharmacokinetic of berberine, the main constituent of Berberis vulgaris L.: a comprehensive review. *Phytother Res*. 2022;36(11):4063–4079. doi:10.1002/ptr.7589
30. Liu L, Xing R, Xue J, et al. Low molecular weight fucoidan modified nanoliposomes for the targeted delivery of the anti-inflammation natural product berberine. *Int J Pharm*. 2023;642:123102. doi:10.1016/j.ijpharm.2023.123102
31. Qi X, Gao C, Yin C, et al. Development of quercetin-loaded PVCL-PVA-PEG micelles and application in inhibiting tumor angiogenesis through the PI3K/Akt/VEGF pathway. *Toxicol Appl Pharmacol*. 2022;437:115889. doi:10.1016/j.taap.2022.115889
32. Zhu C, Gong S, Ding J, et al. Supersaturated polymeric micelles for oral silybin delivery: the role of the Soluplus-PVPVA complex. *Acta Pharm Sin B*. 2019;9(1):107–117. doi:10.1016/j.apsb.2018.09.004
33. Sun F, Zheng Z, Lan J, et al. New micelle myricetin formulation for ocular delivery: improved stability, solubility, and ocular anti-inflammatory treatment. *Drug Deliv*. 2019;26(1):575–585. doi:10.1080/10717544.2019.1622608
34. Hou J, Sun E, Sun C, et al. Improved oral bioavailability and anticancer efficacy on breast cancer of paclitaxel via Novel Soluplus((R))-Solutol((R)) HS15 binary mixed micelles system. *Int J Pharm*. 2016;512(1):186–193. doi:10.1016/j.ijpharm.2016.08.045
35. Poilil Surendran S, George Thomas R, Moon MJ, Jeong YY. Nanoparticles for the treatment of liver fibrosis. *Int J Nanomed*. 2017;12:6997–7006. doi:10.2147/IJN.S145951
36. Gu L, Zhang F, Wu J, et al. Nanotechnology in drug delivery for liver fibrosis. *Front Mol Biosci*. 2021;8:804396. doi:10.3389/fmolb.2021.804396
37. Li Y, Pu S, Liu Q, et al. An integrin-based nanoparticle that targets activated hepatic stellate cells and alleviates liver fibrosis. *J Control Release*. 2019;303:77–90. doi:10.1016/j.jconrel.2019.04.022

38. Lin L. Nanodrug with ROS and pH dual-sensitivity ameliorates liver fibrosis via multicellular regulation. *Adv Sci*. 2020;7(7):1903138. doi:10.1002/advs.201903138
39. Liu X, Li W, Zhang H, et al. Biodistribution and pharmacokinetic profile of berberine and its metabolites in hepatocytes. *Phytomedicine*. 2022;104:154288.
40. Hao Y, Song K, Tan X, et al. Reactive oxygen species-responsive polypeptide drug delivery system targeted activated hepatic stellate cells to ameliorate liver fibrosis. *ACS Nano*. 2022;16:20739–20757. doi:10.1021/acsnano.2c07796
41. Liang Y. Remodeling collagen microenvironment in liver using a biomimetic nano-regulator for reversal of liver fibrosis. *Adv Sci*. 2023;10(18):e2300127. doi:10.1002/advs.202300127
42. Liu G, Wei C, Yuan S, et al. Wogonoside attenuates liver fibrosis by triggering hepatic stellate cell ferroptosis through SOCS1/P53/SLC7A11 pathway. *Phytother Res*. 2022;36(11):4230–4243. doi:10.1002/ptr.7558
43. Roth J, Hoop CL, Williams JK, et al. Probing the effect of glycosaminoglycan depletion on integrin interactions with collagen I fibrils in the native extracellular matrix environment. *Protein Sci*. 2023;32(1):e4508. doi:10.1002/pro.4508
44. Wang X, Wang Q, Liu Z, et al. Preparation, pharmacokinetics and tumour-suppressive activity of berberine liposomes. *J Pharm Pharmacol*. 2017;69(6):625–632. doi:10.1111/jphp.12692